Experimental Analysis of the Multipath Lifetime in Indoor Millimeter-Wave Channels

Mbugua, Allan Wainaina; Chen, Yun; Ji, Yilin; Fan, Wei

Published in:
I E E E Antennas and Wireless Propagation Letters

DOI (link to publication from Publisher):
10.1109/LAWP.2023.3319349

Publication date:
2024

Document Version
Accepted author manuscript, peer reviewed version

Experimental Analysis of the Multipath Lifetime in Indoor Millimeter-Wave Channels

Allan Wainaina Mbugua *Member, IEEE,* Yun Chen *Member, IEEE,* Yilin Ji, and Wei Fan *Senior Member, IEEE*

***Abstract*—Dense spatial sampling of a radio channel where measurements are carried out in many spatial locations is often necessary to accurately capture the multipath components (MPCs) lifetime, i.e. the birth and death process of the MPCs. However, dense spatial sampling is limited by a channel sounder's capabilities such as the number of channel impulse responses (CIRs) per unit time that can be recorded and the measurement duration required to capture the CIRs. The number of spatial samples can be reduced significantly by an interpolation of the channel in a given interval in post-processing. However, interpolation of the channel requires that there is no significant birth and death of the dominant MPCs in the selected interpolation interval. In this letter, a configuration of two antenna arrays is proposed for monitoring the birth and death of MPCs by comparing the frequency correlation signature of the arrays thus enabling a reduction of the density of spatial sampling. This is validated in an indoor scenario at the mm-wave frequency band from 26.5 GHz to 30 GHz along a linear trajectory.**

***Index Terms*—Millimeter-wave, multipath lifetime, radio channel sounding, virtual antenna array.**

I. INTRODUCTION

RADIO channel models are an integral part of the testing and optimization phases of wireless communication systems design. Specifically, in virtual drive testing (VDT), sequences of channel impulse responses (CIRs) along a predefined trajectory are often required in radio channel emulators for this purpose [1]. This can be achieved by conducting extensive measurement campaigns, using ray tracing (RT) simulators e.g. dynamic RT [2], [3] or interpolation of RT simulation outputs [4], [5] or using simulation techniques such as 3GPP channel simulators e.g. QuaDRiGa [6]. However, the birth and death process of multipath components (MPCs) in a radio channel for example due to shadowing especially in millimeter-wave (mm-wave) frequency bands which have a high susceptibility to blockage [7], leads to the need of more spatial samples to accurately capture the MPC lifetime.

In theory, from a ray-optical perspective, to capture the precise location of the appearance or disappearance of an MPC, the spatial separation of the positions along a trajectory should be infinitely small cf. [8, Fig. 1]. Thanks to the sampling theorem, this distance can be increased to half wavelength. However, sampling at the Nyquist rate is still challenging or impractical in both measurement and simulation based channel model development methods. In channel measurements, the limiting factor is the hardware capability of the channel sounding platform such as the switching time of the antenna arrays, the data streaming rate, storage capacity, and the re-calibration or clock re-synchronization time-interval [9]–[11]. In addition, when virtual antenna array or directional scanning with horn antennas are used to obtain the spatial profile of the channel, the measurement time scales up significantly due to the slow speed of the antenna positioners. Furthermore, in vector network analyzer (VNA) based channel sounders, the noise floor is dependent on the intermediate frequency (IF) bandwidth settings. A narrow IF bandwidth results in a lower noise floor and consequently a higher dynamic range compared to a wider IF bandwidth. At mm-wave frequencies, to increase the dynamic range of VNA based channel sounders, it is often necessary to employ a narrow IF bandwidth. However, this further increases the measurement time of these sounders as a narrow IF bandwidth results in a slower frequency sweep compared to a wider IF bandwidth [10], [12].

The reduction of the number of channel spatial samples in a given spatial interval is thus of utmost importance as it dictates the channel measurement or simulation duration. However, the underlying assumption is that the channel is stationary i.e. there is no birth and death of the dominant MPCs in the given spatial interval such that interpolation of the channel can be carried out in post-processing. In the literature, methods of determining the stationarity interval *in situ* i.e. during a measurement campaign in an arbitrary scenario are largely missing. To this end, we propose a measurement setup using at least two virtual uniform rectangular arrays (URAs) for detection of the birth and death of MPCs. The antennas are separated with a suitable distance such that there is minimal mutual coupling between the two antennas. By comparing the inter-element frequency correlation signature of the two URAs, the birth and death of MPCs can be detected thus enabling an adaptive sampling of the channel. Therefore, the number of spatial samples along the section of a given trajectory can potentially be increased when there is birth and death of MPCs or decreased when MPCs are stationary in a given section.

II. PROBLEM STATEMENT

Consider two URAs composed of K omni-directional antenna elements with an inter-element distance of 0.4λ as shown in Fig. 1. The URAs are separated by a distance 50λ where λ denotes the wavelength at the highest frequency. If M locally plane waves impinge on the URAs, the frequency response of the reference element of each array $H(f)$ can be

A. W. Mbugua and Y. Chen are with Huawei Technologies Duesseldorf GmbH, Munich Research Center, Munich, Germany.

Y. Ji and W. Fan are with the Antennas, Propagation and Millimetre-Wave Systems (APMS) Section, Aalborg University, Aalborg, Denmark.

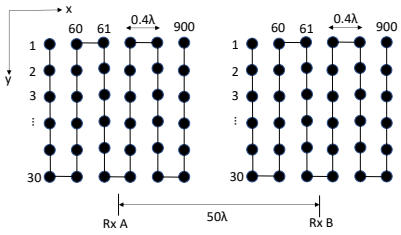

Fig. 1. An illustration of the proposed antenna array configuration setup for monitoring the birth and death of MPCs. It is worthwhile to note that the maximum alias free inter-element distance is 0.5λ.

expressed as:

$$H(f) = \sum_{m=1}^{M} \alpha_m e^{-j2\pi f \tau_m} \tag{1}$$

where α_m and τ_m are the complex amplitude and delay of the m-th plane wave, respectively. The frequency response of the k-th element of each array $H_k(f)$ can be expressed as a phase shifted version of the reference element's frequency response $H(f)$ [13].

$$H_k(f) = \sum_{m=1}^{M} \alpha_m e^{-j2\pi f(\tau_m + \delta_m)} \tag{2}$$

where δ_m is the propagation delay due to the relative position of the k-th element in the array and the angle of arrival (AoA) of the m-th MPC. Using (2), the frequency correlation signature ρ_k for the k-th element to the reference element in the array can then be evaluated by using the frequency response assurance criterion (FRAC) [14]. For example, receiver (Rx) A's frequency correlation signature can be computed as follows:

$$\rho_k^A = \frac{|\sum_{n=1}^{N} H^A(f_n) H_k^{A*}(f_n)|^2}{\sum_{n=1}^{N} H^A(f_n) H^{A*}(f_n) \sum_{n=1}^{N} H_k^A(f_n) H_k^{A*}(f_n)} \tag{3}$$

where N and $(\cdot)^*$ are the number of frequency samples and the Hermitian transpose, respectively. $\rho_k^A \in [0, 1]$ with $\rho_k^A = 1$ indicating a perfect match of the reference element frequency response and the k-th element frequency response. Similarly, the frequency correlation signature for Rx B, ρ_k^B, can be computed using (3).

If the local plane wave fronts observed at the two URAs are the same i.e. the number of local plane waves and the respective AoA, then their respective k-th element frequency correlation signatures are identical i.e. $\rho_k^A = \rho_k^B$. This is based on the condition that the antenna geometry and inter-element spacing is the same and there is no birth and death of MPCs in either of the array. Consider a synthetic case where four MPCs, MPC $1, 2, 3$ and MPC 4, impinge on the URAs shown in Fig. 1 with an azimuth AoA of $212°$, $305°$, $121°$, and $196°$, a delay of 16 ns, 19.9 ns, 27.3 ns, and 33.6 ns, and a magnitude of -66.6 dB, -83.7 dB, -82.8 dB, and -75.5 dB, respectively. This results in a CIR response across the URAs elements as illustrated in Fig. 2(a) and Fig. 2(b) for Rx A and Rx B, respectively. Taking the first antenna element for each URA as the reference element, the frequency correlation signature is computed using (3). Since the two arrays observe the same

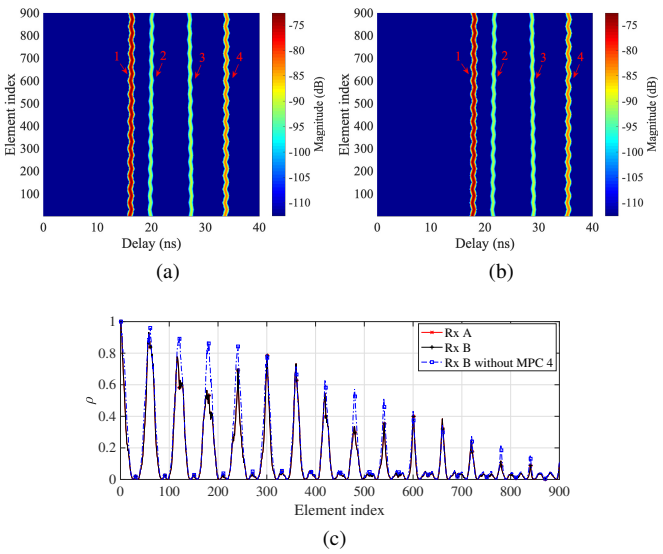

Fig. 2. The CIR per array element across the URAs and the inter-element FRAC for the synthetic case. (a) CIR Rx A. (b) CIR Rx B. (c) Inter-element FRAC where the first antenna in each array is the reference element.

MPCs, the frequency correlation signature is exactly the same as shown in Fig. 2(c). However, when MPC 4 is absent in Rx B while still present in Rx A, the correlation signature differs, indicating a change in the MPC structure in the propagation channel. In both URAs, the frequency correlation signature can also be observed to correspond to the array geometry illustrated in Fig. 1 as it decreases with an increase in the distance from the reference element. Therefore, by comparing the inter-element correlation signature of the two URAs, we can examine the spatial non-stationarity of the channel.

III. MEASUREMENT CAMPAIGN

A measurement campaign is conducted in a meeting room as shown in Fig. 3 and Fig. 4 using the VNA based channel sounder outlined in [15] in the frequency band between 26.5 GHz to 30 GHz, where the transmitter (Tx) [16] and Rx antennas are placed at a height of 1.7 m. The channel sounder employs radio-over-fiber techniques to minimize the signal attenuation in the Tx-Rx chain resulting in a higher dynamic range, thus enabling the identification of weak MPCs. Two vertically polarized bi-conical antennas with an omni-directional pattern in the azimuth are mounted on the same antenna positioner with a separation distance of 50λ at 30 GHz resulting in two virtual URAs at the Rx as shown in Fig. 1. Using this configuration, a measurement campaign is conducted with the Tx at 17 positions as illustrated in Fig. 3. The distance between the Tx positions is approximately 30 cm except between position 16 and 17 where the distance is 20 cm due to proximity of the Tx antenna to the wall. The goal of this measurement setup is to mimic the death and birth of MPCs due to the change in the spatial location of the Tx. Note that in these measurements the channel is kept static in the entire measurement duration. This is due to the fact that radio channel measurements with a VNA in conjunction with

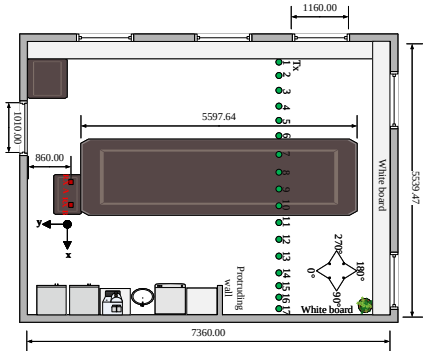

Fig. 3. An illustration of the measurement setup with the considered Tx positions.

(a)

Fig. 4. Panorama photo of the measurement scenario.

virtual antenna arrays requires that the channel is stationary during the time needed to record one channel snapshot.

IV. RESULTS ANALYSIS

In this measurement setup, the first goal is to estimate the individual MPCs at each location. The second goal is to investigate whether the birth and death of the MPCs at each Tx position can be detected based on the frequency correlation signature of the two URAs. The channel multipath parameters i.e. the power, delay, azimuth AoA, and elevation AoA of the MPCs are estimated with the space-alternating generalized expectation-maximization (SAGE) algorithm for each Tx position [17]. The evolution of the MPCs observed at Rx A and Rx B is illustrated in Fig. 5(a) and Fig. 5(b), respectively. In the present work, the identification of MPCs trajectories is done manually, however, automatic identification of the MPCs trajectories can be carried out using various algorithms e.g. Kalman filter based algorithms [7], [18] and references therein. Apart from the offset in delay and angle due to the position of the URAs, most of the MPCs can be observed to have a similar trajectory in the estimated power angle delay profile (PADP) from the two URAs. The geometry of the scenario can partially be observed in the MPCs structure. For instance, the trajectory g can be deduced to be a specular reflected MPCs from the metallic white board parallel to the Tx route cf. Fig. 3. Trajectory j and k are contributions from the windows which are recessed from the metallic white board by about $50\,\text{cm}$. This can be observed from the delay difference of approximately $3.5\,\text{ns}$ between the MPCs at the beginning and the end of trajectory g in comparison to that at the beginning of trajectory j and k.

Although the MPC structure for the dominant paths is relatively similar in most positions, for a given Tx position, some dominant MPCs are observed only in one of the URAs.

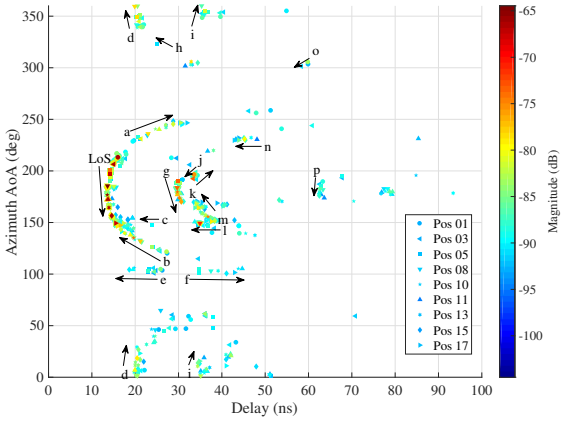

(a)

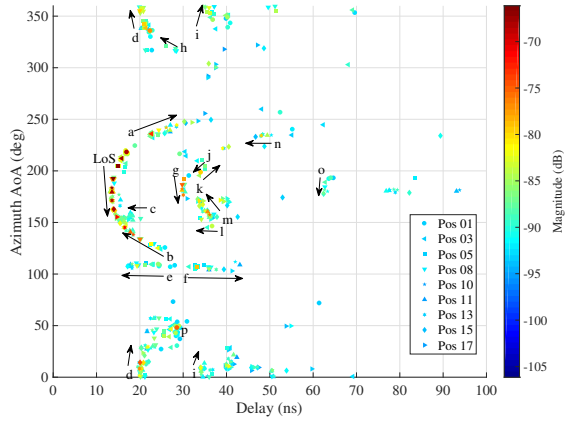

(b)

Fig. 5. The superimposed PADPs for selected Tx positions along the Tx route illustrating the evolution of the MPCs. The arrows indicate the direction of an MPC evolution. (a) The PADP observed at Rx A. (b) The PADP observed at Rx B.

For example, at Tx position 1, a dominant MPC path p in Fig. 5(b) is observed in Rx B only. Similarly, in Tx position 8, a dominant MPC is observed in Rx A in the middle of trajectory l. In Tx position 17, paths to Rx B are partially shadowed by the protruding wall shown in Fig. 3 which causes significant death of MPCs compared to Rx A. In addition, several weak MPCs most probably caused by diffuse scattering can be observed to be present or absent in the PADP observed in both URAs for a given position.

The second goal of this study is to identify the variations in the MPC structure for each Tx position by comparing the frequency correlation signature of the two URAs at the Rx. In principle, the MPCs parameters for each array can be estimated and the differences in MPCs seen by the two arrays can be compared as shown in Fig. 5. However, the accuracy of high resolution channel parameter estimators used to obtain the PADP depends on the validity of several assumptions such as the stationarity of MPCs across the antenna array, the far field assumption, the narrowband assumption which may not be fully satisfied in practical measurements hence leading to inaccurate channel parameter estimates [19], [20]. In addition, high resolution channel parameter estimators for ultra-wideband channels are computationally intensive and

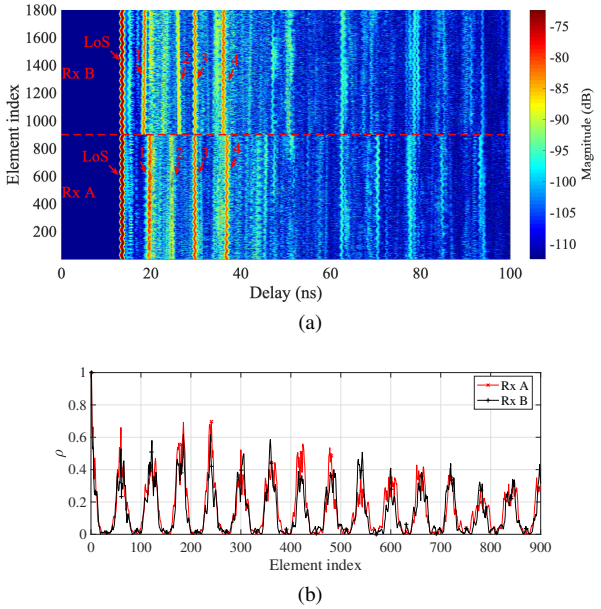

Fig. 6. The CIR per antenna element across the URAs and the inter-element FRAC at Tx position 10. (a) CIR at Rx A (element index 1 to 900) and Rx B (element index 901 to 1800). (b) Inter-element FRAC where the first antenna in each array is the reference element.

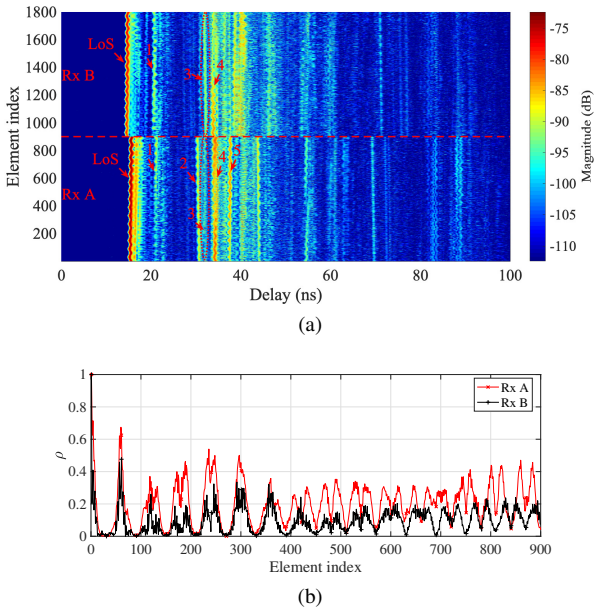

Fig. 7. The CIR per antenna element across the URAs and the inter-element FRAC at Tx position 17. (a) CIR at Rx A (element index 1 to 900) and Rx B (element index 901 to 1800). (b) Inter-element FRAC where the first antenna in each array is the reference element.

thus may not be reliably performed during a measurement campaign, where the measurement time is often limited. This is particularly severe in VNA based channel sounders where the channel must be kept static in the entire measurement duration. On the contrary, the proposed approach using the frequency correlation signature potentially indicates two types of non-stationarity in the channel due to the birth and death of MPCs. First, the MPC may be non-stationary in either or both URAs, i.e. some MPCs may not be visible in all elements in the antenna array and second, some MPCs may be partially or completely missing in one array and present in the other. This information can thus be used to adjust the distance between Tx positions (cf. Fig. 3) i.e. a larger distance can be employed when no significant birth and death of MPCs is observed.

For example, at Tx position 10, the dominant MPCs across the URAs i.e. the line-of-sight (LoS) component and path 1 to 4 are relatively similar as shown in Fig. 6(a). This can be observed in the frequency correlation signature of the two URAs in Fig. 6(b). Despite the similarity, an exact match is not obtained. This is most probably due to diffuse scattered paths in this frequency band which contribute to the weaker paths observed Fig. 6(a). These paths cause differences in the MPC structure in the two URAs which are also manifested in the frequency correlation signatures. At Tx position 17, Rx B is partially shadowed by the protruding wall in the scenario as shown in Fig. 3. This can be observed in the CIR of Rx A and Rx B in Fig. 7(a) where path 2 and 5 are missing in Rx B whereas path 4 is non-stationary across Rx B. These differences in the MPC structure are expected to cause differences in the frequency correlation signature which is exhibited in Fig. 7(b). The larger dissimilarity of the MPCs structure at Tx position 17 compared to position 10 can also be seen in the larger deviations of the frequency correlation signature at this position. This implies that in the vicinity of Tx position 17, more spatial samples are required to accurately capture the birth and death of MPCs. On the other hand, in the vicinity of Tx position 10, coarse spatial sampling can employed. This is because the channel exhibits a high similarity at two observations points separated by 50λ at 30 GHz.

V. CONCLUSION

In this letter, a channel sounding configuration using two virtual URAs has been demonstrated to be a potential solution for the detection of the MPCs birth and death process in radio channels *in-situ*. By observing the differences in the frequency correlation signature for the two URAs for a given location, possible birth and death of dominant MPCs can be detected. Consequently, a coarse sampling of the channel can be carried out where the channel exhibits a high similarity and fine sampling can be used in spatial locations where the channel exhibits a high dissimilarity. This has an important implication since reducing the number of channel measurements required to evaluate the evolution of MPCs results in a measurement time reduction. Although a similarity of the channel can be evaluated by comparing the PADP from the antenna arrays, the advantage of the proposed method is that it computationally efficient hence can be performed on site during a measurement campaign. Furthermore, the accuracy of proposed method is not dependent on MPCs stationarity across the array elements which is often assumed in channel parameter estimation algorithms. In light of the deviations in the frequency correlation signature caused e.g. by diffuse scattered paths, future work will focus on the determination of the appropriate threshold to determine when the spatial sampling rate should be increased or decreased. In addition, the applicability of the proposed method in dynamic scenarios will be studied using a real-time channel sounder and real antenna arrays.

REFERENCES

[1] A. W. Mbugua, Y. Chen, L. Raschkowski, Y. Ji, M. Gharba, and W. Fan, "Efficient Preprocessing of Site-Specific Radio Channels for Virtual Drive Testing in Hardware Emulators," *IEEE Trans. Aerosp. Electron. Syst.*, vol. 59, no. 2, pp. 1787–1799, 2023.

[2] D. Bilibashi, E. M. Vitucci, and V. Degli-Esposti, "Dynamic Ray Tracing: Introduction and Concept," in *Proc. 14th Eur. Conf. Antennas Propag. (EuCAP)*, 2020, pp. 1–5.

[3] F. Quatresooz, S. Demey, and C. Oestges, "Tracking of Interaction Points for Improved Dynamic Ray Tracing," *IEEE Trans. Veh. Technol.*, vol. 70, no. 7, pp. 6291–6301, 2021.

[4] R. Zentner and A. K. Mucalo, "Ray tracing interpolation for continuous modeling of double directional radio channel," in *Proc. Eurocon*, 2013, pp. 212–217.

[5] J. Nuckelt, M. Schack, and T. Kürner, "Geometry-Based Path Interpolation for Rapid Ray-Optical Modeling of Vehicular Channels," in *Proc. 9th Eur. Conf. Antennas Propag. (EuCAP)*, 2015, pp. 1–5.

[6] S. Jaeckel, L. Raschkowski, K. Börner, and L. Thiele, "QuaDRiGa: A 3-D Multi-Cell Channel Model With Time Evolution for Enabling Virtual Field Trials," *IEEE Trans. Antennas Propag.*, vol. 62, no. 6, pp. 3242–3256, 2014.

[7] C. Lai, R. Sun, C. Gentile, P. B. Papazian, J. Wang, and J. Senic, "Methodology for Multipath-Component Tracking in Millimeter-Wave Channel Modeling," *IEEE Trans. Antennas Propag.*, vol. 67, no. 3, pp. 1826–1836, 2019.

[8] S. Hussain and C. Brennan, "Efficient Preprocessed Ray Tracing for 5G Mobile Transmitter Scenarios in Urban Microcellular Environments," *IEEE Trans. Antennas Propag.*, vol. 67, no. 5, pp. 3323–3333, 2019.

[9] Z. Wen and H. Kong, "mmWave MIMO Channel Sounding for 5G," in *Proc. 1st Int. Conf. 5G Ubiquitous Connectivity*, 2014, pp. 192–197.

[10] G. R. MacCartney and T. S. Rappaport, "A Flexible Millimeter-Wave Channel Sounder With Absolute Timing," *IEEE J. Sel. Areas Commun.*, vol. 35, no. 6, pp. 1402–1418, June 2017.

[11] C. U. Bas, R. Wang, S. Sangodoyin, D. Psychoudakis, T. Henige, R. Monroe, J. Park, C. J. Zhang, and A. F. Molisch, "Real-Time Millimeter-Wave MIMO Channel Sounder for Dynamic Directional Measurements," *IEEE Trans. Veh. Technol.*, vol. 68, no. 9, pp. 8775–8789, 2019.

[12] A. W. Mbugua, W. Fan, Y. Ji, and G. F. Pedersen, "Millimeter Wave Multi-User Performance Evaluation Based on Measured Channels With Virtual Antenna Array Channel Sounder," *IEEE Access*, vol. 6, pp. 12 318–12 326, 2018.

[13] L. Godara, "Application of Antenna Arrays to Mobile Communications. II. Beam-forming and Direction-of-Arrival Considerations," *Proc. IEEE*, vol. 85, no. 8, pp. 1195–1245, 1997.

[14] W. Heylen and S. Lammens, "FRAC: A Consistent Way of Comparing Frequency Response Functions," in *Proc. Conf. Identification Eng. Syst.*, 1996, pp. 48–57.

[15] A. W. Mbugua, W. Fan, K. Olesen, X. Cai, and G. F. Pedersen, "Phase-Compensated Optical Fiber-Based Ultrawideband Channel Sounder," *IEEE Trans. Microw. Theory Techn.*, vol. 68, no. 2, pp. 636–647, 2020.

[16] S. S. Zhekov, A. Tatomirescu, and G. F. Pedersen, "Antenna for Ultrawideband Channel Sounding," *IEEE Antennas Wireless Propag. Lett.*, vol. 16, pp. 692–695, 2017.

[17] B. H. Fleury, M. Tschudin, R. Heddergott, D. Dahlhaus, and K. I. Pedersen, "Channel Parameter Estimation in Mobile Radio Environments Using the SAGE Algorithm," *IEEE J. Sel. Areas Commun.*, vol. 17, no. 3, pp. 434–450, March 1999.

[18] K. Mahler, W. Keusgen, F. Tufvesson, T. Zemen, and G. Caire, "Tracking of Wideband Multipath Components in a Vehicular Communication Scenario," *IEEE Trans. Veh. Technol.*, vol. 66, no. 1, pp. 15–25, 2017.

[19] Y. Ji, W. Fan, and G. F. Pedersen, "Channel Characterization for Wideband Large-Scale Antenna Systems Based on a Low-Complexity Maximum Likelihood Estimator," *IEEE Trans. Wireless Commun.*, vol. 17, no. 9, pp. 6018–6028, 2018.

[20] F. Zhang and W. Fan, "Near-Field Ultra-Wideband mmWave Channel Characterization Using Successive Cancellation Beamspace UCA Algorithm," *IEEE Trans. Veh. Technol.*, vol. 68, no. 8, pp. 7248–7259, 2019.